

# *Ab initio* analysis of electron-phonon coupling in molecular devices

N. Sergueev, D. Roubtsov, and Hong Guo

*Center for the Physics of Materials and Department of Physics,*

*McGill University, Montreal, PQ, Canada, H3A 2T8*

## Abstract

We report first principles analysis of electron-phonon coupling in molecular devices under external bias voltage and during current flow. Our theory and computational framework are based carrying out density functional theory within the Keldysh nonequilibrium Green's function formalism. We analyze which molecular vibrational modes are most relevant to charge transport under nonequilibrium conditions. For a molecular tunnel junction of a 1,4-benzenedithiolate molecule contacted by two leads, the low-lying modes of the vibration are found to be most important. As a function of bias voltage, the electron-phonon coupling strength can change drastically while the vibrational spectrum changes at a few percent level.

PACS numbers: 81.07.Nb, 68.37.Ef, 72.10.-d, 73.63.-b

One of the most important questions concerning charge transport in molecular electronic devices is the role of electron-phonon (e-p) interaction. Here, “phonon” refers to quantized molecular vibrational modes which couple to various scattering states of the device. A typical molecular device has the Metal-Molecule-Metal (MMM) configuration schematically shown in Fig. 1, where metal leads extend to far away and bias voltages can be applied so that a current flows through. The problem of predicting vibrational spectra and e-p coupling strength for such an open system during current flow, within self-consistent first principles including all atomic details of the molecule as well as the leads, is a serious theoretical challenge that has not been satisfactorily addressed. A particularly important problem is to understand which vibrational mode couples to which scattering state at what bias voltage [1, 2]. It is the purpose of this article to address this issue.

Experimentally, single molecule vibrational spectra can be measured by inelastic tunneling spectroscopy (IETS) [3, 4, 5]. Theoretically, various models have been applied to understand IETS and to investigate effects of e-p interaction based on tight binding atomistic Hamiltonians [6, 7, 8]. Recently, Frederiksen *et al.* [9] reported a first principles analysis of inelastic current due to e-p interactions in an Au chain, in which the relevant vibrations are along the chain length. In their theory [9], the vibrational spectra was obtained using a plane-wave basis density functional theory (DFT) code in a cluster configuration at equilibrium, and the dynamic matrix was evaluated using a finite differencing scheme. Transport properties were then obtained using the Transiesta package [10] with LCAO basis, and e-p scattering was included at the level of self-consistent Born approximation.

In order to investigate voltage dependence of the e-p interaction in MMM devices, however, quantized molecular vibrations and electrons need to be treated on equal footing at *nonequilibrium*. We accomplish this by carrying out DFT atomic analysis within the Keldysh nonequilibrium Green’s function (NEGF) formalism [11]. In addition, we calculate the dynamic matrix within the NEGF-DFT formalism [11] by evaluating analytical formula rather than numerical finite differencing [9]: this is more general and more accurate so that all the phonon modes and e-p couplings can be obtained for complicated systems. For a molecular tunnel junction of a 1,4-benzenedithiolate (BDT) molecule contacted by two metallic electrodes (see Fig. 1), we found that the low-lying modes of the vibration are the most important for e-p coupling. As a function of bias voltage, the coupling strength can change drastically while the vibrational spectrum changes at a few percent level.

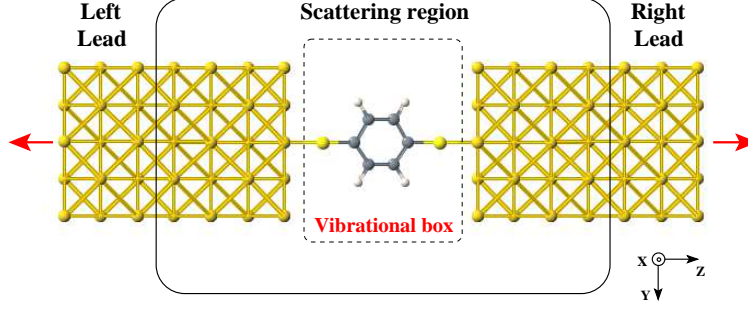


FIG. 1: Schematic plot of an Metal-BDT-Metal molecular tunneling junction (BDT =  $C_6H_4S_2$ ). The electrodes consist of repeated unit cells extending to  $z = \pm\infty$ . The scattering region contains several layers of electrodes and the molecule. The vibrational box lies inside the scattering region.

We start from the NEGF-DFT formalism documented in Ref. 11, in which the density matrix  $\hat{\rho}$  is calculated by NEGF  $G^<$ ,  $\hat{\rho} \sim \int dE G^<(E)$ . This way, we naturally take into account external bias voltage and open device transport boundary condition. After the Kohn-Sham Hamiltonian  $\hat{H}_{KS}[\hat{\rho}]$  of the device is obtained self-consistently, the total energy of the scattering region (see Fig. 1), as well as all transport properties of the device, can be obtained [11]. Importantly, the NEGF-DFT formalism allows one to obtain  $\hat{H}_{KS}$  and total energy  $E(\{\mathbf{R}_i\}, V_b)$  as functions of external bias  $V_b$ , ( $\mathbf{R}_i$  is the position of the  $i$ -th atom).

The phonon (vibrational) eigenvectors  $\mathbf{e}_\nu$  and frequencies  $\omega_\nu$  ( $\nu$  is the mode index) are obtained by diagonalizing the dynamic matrix (Hessian matrix),

$$\mathcal{H}_{j,j'} = \nabla_{\mathbf{R}_j} \nabla_{\mathbf{R}_{j'}} E(\{\mathbf{R}_i\}, V_b) / \sqrt{M_j M_{j'}}, \quad (1)$$

where  $M$  is the mass of an atom. Once  $(\mathbf{e}_\nu, \omega_\nu)$  are obtained, the e-p interaction strength  $g^\nu$ , defined by the e-p Hamiltonian [12], can be obtained from the standard expression:

$$g_{j,\mu;j',\mu'}^\nu = \sum_i \sqrt{\frac{\hbar}{2M_i\omega_\nu}} \mathbf{e}(\nu, i) \langle \phi_{j,\mu} | \nabla_{\mathbf{R}_i} \hat{H}_{KS} | \phi_{j',\mu'} \rangle. \quad (2)$$

Here,  $|\phi_{j,\mu}\rangle$  is a basis function for orbital  $\mu$  ( $\mu = s, p, d$ ) of the  $j$ -th atom. The derivative of the KS Hamiltonian is carried out by fixing the atomic positions at their stationary locations  $\mathbf{R}_i^0$ . ( $\mathbf{R}_i^0$  is where the  $i$ -th atom feels no force [13].) Although the Hessian matrix  $\mathcal{H}_{j,j'}$  and the e-p coupling matrix  $g_{j,\mu;j',\mu'}^\nu$  appear to have the same form as those for equilibrium system, the derivatives of  $\hat{H}_{KS}(\{\mathbf{R}_i\}, V_b)$  and  $E(\{\mathbf{R}_i\}, V_b)$  with respect to  $\mathbf{R}_i$  propagate to derivatives of NEGF  $G^<(E)$  that includes nonequilibrium physics [13].

The e-p coupling is characterized by a dimensionless parameter [12]  $\lambda_{e-p}$  which is contributed by all phonon modes,

$$\lambda_{e-p} = \sum_{\nu} \lambda_{\nu}, \quad \lambda_{\nu} \equiv DOS(\varepsilon_F) \frac{|\langle g^{\nu} \rangle|^2}{\hbar\omega_{\nu}}. \quad (3)$$

Here,  $DOS(E)$  is the density of states of the scattering region and  $\varepsilon_F$  the Fermi energy of the leads. As we are interested in e-p coupling for quantum transport, the  $g^{\nu}$  matrix is averaged over scattering states  $\Psi_{sc}$ , which are obtained by the NEGF-DFT numerical package [11] for any MMM device:

$$\langle g^{\nu}(E, E') \rangle = \langle \Psi_{sc}(E) | g^{\nu} | \Psi_{sc}(E') \rangle. \quad (4)$$

If both scattering states have the same energy  $E = E' = \varepsilon_F$ , we call such an e-p coupling the “elastic” one,  $\lambda_{\nu}^{el}$ . When  $E = \varepsilon_F$  and  $E' = \varepsilon_F \pm \hbar\omega_{\nu}$ , we call it the “inelastic”  $\lambda_{\nu}^{\pm}$ . Finally, when the MMM device is under an external bias voltage  $V_b$ , we further average  $\lambda_{\nu}$  over the transport energy window  $(\mu_L, \mu_R)$  where  $\mu_{R/L}$  are the electrochemical potentials of the right/left leads and  $|\mu_R - \mu_L| = eV_b$ . Hence, at nonequilibrium, we obtain

$$\lambda_{\nu}^{el}(V_b) = \int_{\mu_L}^{\mu_R} \frac{dE}{eV_b} DOS(E) \frac{|\langle g^{\nu}(E, E) \rangle|^2}{\hbar\omega_{\nu}}. \quad (5)$$

The inelastic coupling  $\lambda_{\nu}^{\pm}(V_b)$  is calculated by replacing  $g^{\nu}(E, E)$  with  $g^{\nu}(E, E \pm \hbar\omega_{\nu})$  in Eq. (5).

The above theoretical formalism is implemented into our NEGF-DFT package McDCAL [11]. In numerical calculations, we further define a “vibrational box” inside the MMM device (see Fig. 1) which contains the atoms of interest. Typically, the vibrational box include the molecule and perhaps a few layers of the nearest lead atoms. The atomic indexes in the above formalism refer to those inside the vibrational box.

In the following, we investigate general features of vibrational spectra and e-p coupling during nonequilibrium transport using the model MMM device of Fig. 1, *i.e.*, a BDT molecular wire [14]. For each bias voltage, we iterate the KS Hamiltonian of the device to numerical convergence using the NEGF-DFT method [11]; the atomic positions in the scattering region must also be relaxed for each applied bias. Afterward, the vibrational spectrum and the e-p coupling are obtained. As a check, we calculated  $\omega_{\nu}$  of an isolated BDT using our NEGF-DFT formalism and obtained reasonable agreement, to within  $\leq 5 - 6$  %,

with experimental data collected by Raman spectroscopy and other methods [15]. We also checked that the *diagonal* matrix elements of the e-p coupling are non-zero for modes having the  $A_g$  symmetry and are zero for other modes, in agreement with selection rules from group theory [16].

When the BDT is placed between the leads (see Fig. 1), new properties arise. First, several low-lying modes that do not exist for isolated BDT are found to play important roles. These modes include the center-of-mass and libration ( $CM(i)$  and  $LB(i)$ ,  $i = X, Y, Z$ ) with energy  $\hbar\omega_\nu \simeq 8 - 14$  meV. Clearly, the presence of leads breaks the translational and rotational symmetries and produces these low-lying modes. Second, many vibrational frequencies are renormalized, to  $\simeq 10 - 30$  %, from that of the isolated molecule. This is especially true for modes with strong sulphur oscillations in the BDT. For large bias,  $V_b \approx 1$  V, we found that  $\omega_\nu$  changes up to 2 % while  $e_\nu$  changes up to 5 % compared with the vibrational spectrum at  $V_b = 0$ . At  $V_b = 0$ , it turns out that all the modes can be classified by the same  $D_{2h}$  point group as in the case of an isolated BDT; at  $V_b \neq 0$ , they can be classified by the  $C_{2v}$  point group.

Fig. 2 plots the e-p coupling  $\lambda_\nu$  versus  $\hbar\omega_\nu$  at  $V_b = 0$ . For small bias voltages,  $V_b \leq 0.5$  V,  $\lambda_\nu$  does not change qualitatively. Most clearly shown is that some phonon modes give distinctly larger e-p coupling to scattering states than others (see Eq. (4)). Beside the expected in-plane  $A_g(n)$  modes, modes of other symmetries are also responsible for the peaks in  $\lambda_\nu$  (see the right insets of Fig. 2 for a few important modes). Notable are the in-plane modes  $B_{1u}(n)$ , the center-of-mass mode  $CM(Z)$ , the out-of-plane modes  $A_u(n)$ ,  $B_{1g}(1)$ , and the libration  $LB(Z)$ . Recall that for vibrational spectroscopy on free BDT such as Raman or infrared, there are always selection rules of modes [15]. For a BDT device, however, our results suggest that no obvious selection rules are followed because many modes with very different symmetries manifest. Interestingly, among the low-lying modes with  $\omega_\nu < 1000$   $\text{cm}^{-1}$  ( $\hbar\omega_\nu < 0.12$  eV), the “breathing” modes  $A_g(1)$  and  $A_g(2)$  are not the most important ones for coupling to scattering states ( $\lambda_\nu \simeq 1 - 2 \times 10^{-4}$ ), although these modes are important for a free BDT. For the BDT device, the total e-p coupling (see Eq. (3)) is  $\lambda_{e-p}^{el} \approx \lambda_{e-p}^- \approx 7 \times 10^{-3}$  at  $V_b = 0$ .

To understand why modes with symmetry other than  $A_g$  can couple to scattering states, as shown by some of the peaks in Fig. 2, we consider Eq. (4). For a *free* BDT, the electronic wave function in Eq. (4) is a molecular orbital, and for each orbital one obtains

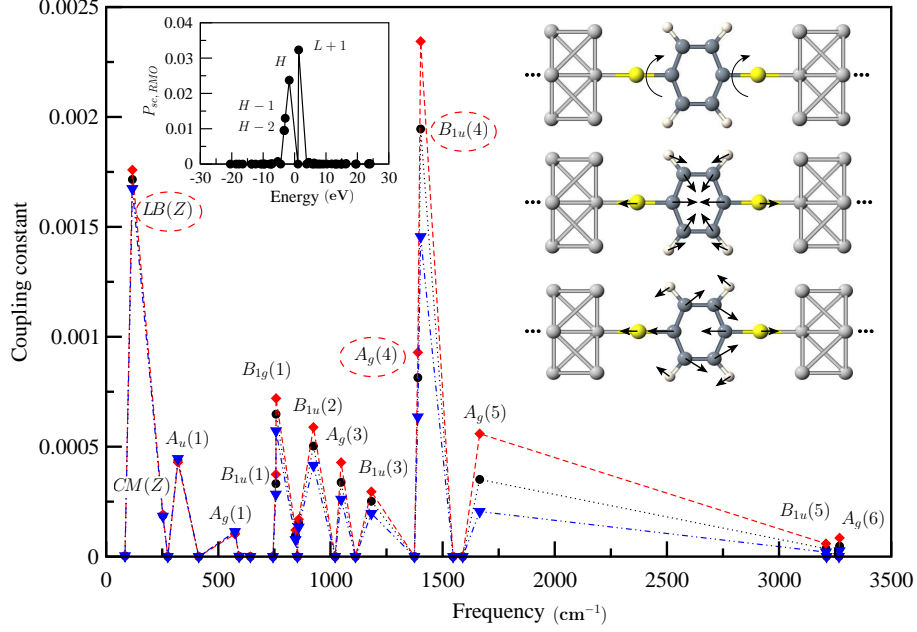


FIG. 2: Dimensionless e-p coupling constants  $\lambda_{\nu}^{el}$  (circles),  $\lambda_{\nu}^{-}$  (triangles),  $\lambda_{\nu}^{+}$  (diamonds) as a function of vibrational frequency  $\omega_{\nu}$  at  $V_b = 0$ . The lines are guide to the eye. The modes are classified using the  $D_{2h}$  point group. The left inset shows projection  $P_{sc,RMO}$  of a scattering state at Fermi energy (shifted to zero) onto molecular orbitals (RMO) of the BDT. Letters  $H$  and  $L$  mean HOMO and LUMO. In the right side insets, we show eigenvectors of several important eigenmodes of the BDT at small biases, namely, the libration  $LB(Z)$  (top),  $A_g(4)$  (middle), and  $B_{1u}(4)$  (bottom).

a value  $\langle g^{\nu} \rangle$ . Hence for a free BDT the relevant e-p coupling is a diagonal matrix in orbital space: only those vibrational modes with  $A_g$  symmetry give nonzero values to these diagonal matrix elements [16]. For transport, however, the wave function appearing in Eq. (4) is a scattering state which is roughly a linear combination of many molecular orbitals. Therefore it is possible to have off-diagonal matrix elements in the coupling matrix so that modes with symmetries other than  $A_g$  can also contribute. This can be substantiated as follows. We project scattering states  $\Psi_{sc}(E)$  onto “renormalized molecular orbitals” (RMO) of the BDT in the MMM device [17].

The RMO’s are obtained by diagonalizing the Hamiltonian sub-matrix that corresponds to the BDT molecule, and this sub-matrix is a part of the total KS Hamiltonian of the entire MMM device [17]. Note that RMO’s can be different from the original molecular orbitals

of an isolated BDT due to charge transfer from the leads to the molecule and external bias potentials. The projection is characterized by the quantity  $P_{sc, RMO} \equiv |\langle \Psi_{sc}(\varepsilon_F) | RMO \rangle|^2$  plotted in the left inset of Fig. 2 as a function of energy. We found that all scattering states  $\Psi_{sc}$  near the Fermi energy are contributed by the *same several* dominant RMO's at low bias. Therefore one can well consider that  $\Psi_{sc}$  is a linear combination of these few RMO's and  $g^\nu$  of Eq. (4) is contributed mostly by them, *i.e.*,  $\langle g^\nu \rangle$  is contributed by a quantity  $g'_{\alpha\alpha'} \equiv \langle RMO_\alpha | g^\nu | RMO_{\alpha'} \rangle$ . Hence, for transport problems, the off-diagonal contributions (when  $\alpha \neq \alpha'$ ) can be as important as the diagonal ones ( $\alpha = \alpha'$ ). Furthermore, when bias  $V_b$  is increased, molecular orbitals in the MMM device [17] become less symmetric so that vibrational modes different from the  $A_g$  symmetry can even contribute to the diagonal matrix elements of the e-p coupling. For example, at  $V_b = 1$  V, the contribution of orbitals HOMO  $- n$  with  $n = 1, 3$  to the scattering states is found to give rise to non-zero e-p coupling for vibrational modes with both the  $A_g$  and  $B_{1u}$  symmetries. These results allow us to conclude that e-p coupling in MMM devices during current flow ( $V_b \neq 0$ ) is much more complicated than that for free molecules.

A most important finding is that at large bias voltage,  $V_b \simeq 1$  V, the e-p coupling strength changes drastically although the vibrational spectrum is only changed by a few percent as mentioned above. Fig. 3 plots the coupling strength at  $V_b = 1$  V. We observe that contributions to e-p coupling are now dominated by a few low-lying modes such as the center-of-mass modes; the total coupling is a factor of five greater than that at low bias (see Fig. 2), and coupling due to individual low-lying modes is also much larger. By projecting different scattering states  $\Psi_{sc}(E)$  with the same energy  $E$  onto RMO's as presented above, we found that two patterns of  $P_{sc, RMO}$  occur, as shown in the left insets of Fig. 3. This indicates that scattering states inside the transport energy window are different from those at low bias. In particular, the pattern of  $P_{sc, RMO}$  in the upper panel is similar to that in Fig. 2, but the new (lower) pattern of  $P_{sc, RMO}$  comes from lower HOMO  $- n$  and higher LUMO  $+ n$  RMO's. This leads to a different behavior of e-p couplings at large biases for the BDT device. For example, our calculations reveal that the peak labeled  $CM(Y)$  in  $\lambda_\nu(\omega_\nu)$  (see Fig. 3) comes from particular off-diagonal matrix elements,  $\langle L + 2 | g^\nu | H - 1 \rangle$  and  $\langle L + 4 | g^\nu | H - 1 \rangle$ . The peak labeled  $CM(Z)$ , on the other hand, is found to come from diagonal matrix elements, *e.g.*,  $\langle H - 1 | g^\nu | H - 1 \rangle$ . These findings also correlate well with the peaks of  $P_{sc, RMO}$  in the left insets of Fig. 3. The total  $\lambda_{e-p}$  at  $V_b \simeq 1$  V is found to

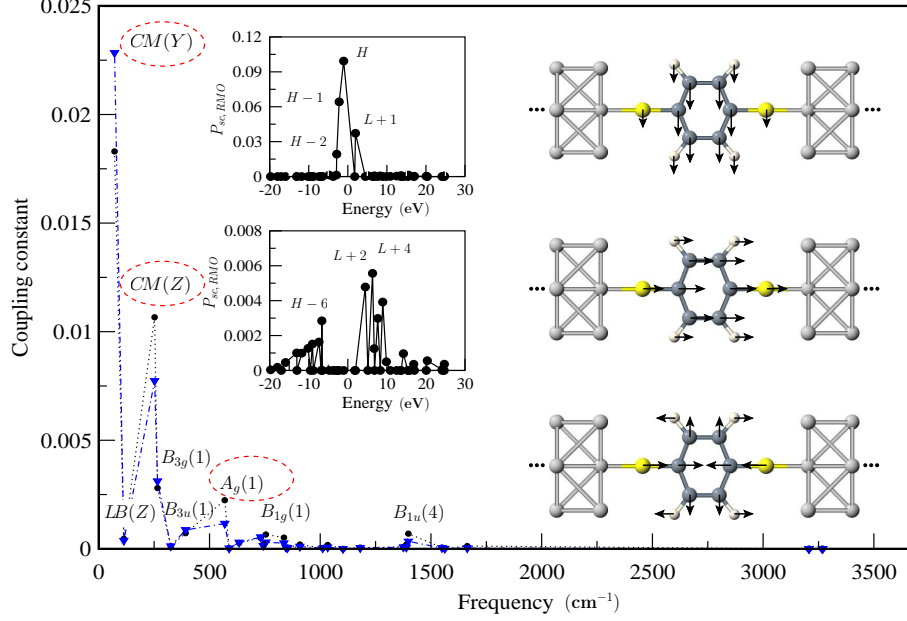


FIG. 3: Dimensionless e-p coupling constants  $\lambda_\nu^{el}$  (circles) and  $\lambda_\nu^-$  (triangles) at  $V_b = 1$  V. Although in principle one should use the  $C_{2v}$  point group to label the modes, for comparison with Fig. 2 we keep the  $D_{2h}$  labels here. The left insets show projection  $P_{sc,RMO}$  for two scattering states taken at  $E - \varepsilon_F = 0.4$  eV. In the right side insets, we show eigenvectors of several important modes at  $V_b \simeq 1$  V, namely,  $CM(Y)$  (top),  $CM(Z)$  (middle), and  $A_g(1)$  (bottom).

be  $\simeq 0.04$ . This enhancement by roughly a factor of five from that of  $V_b \simeq 0$  is due to the center-of-mass modes shown in Fig. 3 that can be confirmed by computing  $\lambda_{e-p}$  without counting these modes.

Why bias voltage can change e-p coupling so drastically? We found that the reason is mainly due to contribution of different scattering states. In the inset of Fig. 4, we plot transmission coefficient  $T(E, V_b)$  vs. electron energy  $E$  for several values of  $V_b$ . Most clearly shown is that  $V_b$  shifts the transmission features toward the transport window. In particular, a sharp peak (at  $E \approx -0.3$  eV) is shifted up-wards in energy with the increase of  $V_b$ . When  $V_b > 0.5$  V, the “tail” of this sharp peak starts entering the transport window (between  $\mu_L = 0$  and  $\mu_R = eV_b$ , see also Eq. (5)). If  $V_b > 0.75$  V, this peak enters into the transport window completely. When this happens, the e-p coupling changes drastically and the new pattern appears in the projection  $P_{sc,RMO}$  as discussed above. Fig. 4 plots the e-p coupling strength  $\lambda_\nu$  for several vibrational modes  $\nu$  and the total  $\lambda_{e-p}$  vs.  $V_b$ . The curves give a

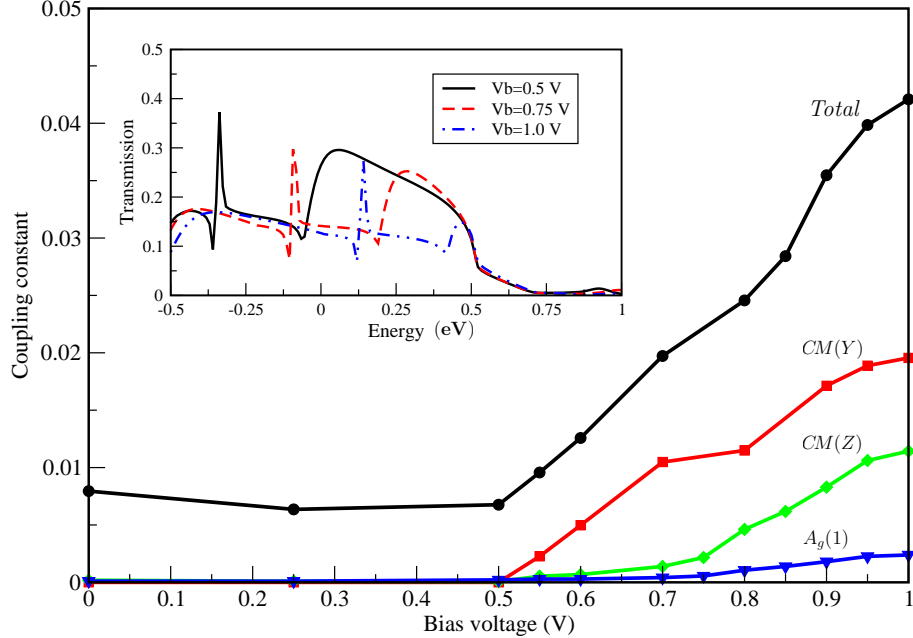


FIG. 4: Dimensionless e-p coupling constants  $\lambda_{e-p}^{el}$  (circles) and  $\lambda_{\nu}^{el}$ , for  $\nu = CM(Y)$  (squares),  $CM(Z)$  (diamonds), and  $A_g(1)$  (triangles), as a function of  $V_b$ . Inset: transmission function  $T(E, V_b)$  at  $V_b = 0.5$  V (full line),  $V_b = 0.75$  V (dashed line), and  $V_b = 1$  V (dash-dot line). The transport energy window ( $\mu_L, \mu_R$ ) lies in the positive part of the energy axis, from  $E = 0$  to  $E = |eV_b|$ .

clear indication that the e-p coupling is roughly a constant at small biases, but can change *nonlinearly* as the applied bias voltage is varied. Such a change can have deep implications to local heating in the device during nonequilibrium charge transport [6, 9, 18, 19].

In summary, the entire relevant vibrational spectrum of a molecule device can be obtained at non-zero bias within the NEGF-DFT formalism where both vibrational and electronic properties are calculated at equal footing. For a 1,4-BDT molecular device studied here, low-lying vibrational modes play an important role in contributing to the e-p coupling strength. The coupling strength changes drastically as bias voltage is increased due to participations of new scattering states. For the BDT device, at large bias of  $V_b \simeq 1$  V, it is the center-of-mass modes which denominate the e-p coupling, while for small bias  $V_b < 0.5$  V, many modes of different symmetries contribute. The vibrational spectrum also depends on bias, but for the BDT device this dependence is at a few percent level.

This work is supported by NSERC of Canada, FQRNT of Québec, and CIAR.

- 
- [1] N. Lorente and M. Persson, Phys. Rev. Lett. **85**, 2997 (2000);  
N. Lorente, M. Persson, L. J. Lauhon and W. Ho, Phys. Rev. Lett. **86**, 2593 (2001).
- [2] M. J. Montgomery, J. Hoekstra, T. N. Todorov and A. P. Sutton, J. Phys.: Condens. Matter **15**, 731 (2003).
- [3] W. Ho, J. Chem. Phys. **117**, 11033 (2002).
- [4] W. Wang, T. Lee, I. Kretzschmar and M. A. Reed, Nano Lett. **4**, 643 (2004).
- [5] Y. Selzer, L. Cai, M. A. Cabassi, Y. Yao, J. M. Tour, T. S. Mayer, D. L. Allara, Nano Lett. **5**, 61 (2005).
- [6] M. J. Montgomery and T. N. Todorov, J. Phys.: Condens. Matter **15**, 8781 (2003).
- [7] M. Galperin, M. Ratner and A. Nitzan, J. Chem. Phys. **121**, 11965 (2004).
- [8] Y. Asai, Phys. Rev. Lett. **93**, 246102 (2004).
- [9] T. Frederiksen, M. Brandbyge, N. Lorente, and A.-P. Jauho, Phys. Rev. Lett. **93**, 256601 (2004).
- [10] M. Brandbyge, J.-L. Mozos, P. Ordejón, J. Taylor, and K. Stokbro, Phys. Rev. B **65**, 165401 (2002).
- [11] J. Taylor, H. Guo, and J. Wang, Phys. Rev. B **63**, 245407 (2001).
- [12] O. Gunnarsson, Rev. Mod. Phys. **69**, 575 (1997).
- [13] For Hessian matrix, the main difficulty is to obtain the double derivative of the Hartree and exchange-correlation energies which are functionals of charge density that in turn depends on bias voltages. These derivatives can be obtained within the NEGF technique.
- [14] In the model calculation, the two identical Al leads contact the molecule by a distance of 2 Å. The leads have a finite cross section oriented in the (100) direction with nine atoms per unit cell and extend to  $z = \pm\infty$ . The vibrational box includes the molecule. A single zeta  $s, p, d$  basis set is used in the NEGF-DFT self-consistent calculations.
- [15] S. H. Cho H. S. Han, D.-J. Jang, K. Kim, and M. S. Kim, J. Phys. Chem. **99**, 10594 (1995);  
S. W. Joo, S. W. Han, and K. Kim, J. Coll. Interf. Sci. **240**, 391 (2001).
- [16] M. Tinkham, *Group Theory and Quantum Mechanics* (McGraw-Hill, New York, 1964).
- [17] B. Larade, J. Taylor, Q. R. Zheng, H. Mehrez, P. Pomorski, and H. Guo, Phys. Rev. B **64**, 195402 (2001).

- [18] Y.-C. Chen, M. Zwolak, and M. Di Ventra, *Nano Lett.* **3**, 1691 (2003); *ibid.* **4**, 1709 (2004).
- [19] Z. Yang, M. Chsiev, M. Zwolak, Y.-C. Chen, and M. Di Ventra, *Phys. Rev. B* **71**, 041402 (2005).